The progressive crystallization and ordering of low-temperature dolomites

HARTMUT SCHNEIDER

Mineralogisches Institut der Universität Karlsruhe, Germany

SUMMARY. The progressive crystallization of dolomite has been investigated in the temperature range of 90 to 410 °C by means of X-ray powder diffraction, electron microscopy, and infra-red spectroscopy.

Short-time, low-temperature experiments ($\leqslant$ 145 °C) yielded dolomites with a high defect density. In detail, lattice faults can be described as: Random succession of more or less ordered cation domains, producing a long-range mosaic-type disorder; cation ordering may take place along $\langle 10\bar{1}0 \rangle$ and $\langle 11\bar{2}0 \rangle$; tilting and dislocation of individual CO_3 groups; and irregular interstratification of dolomite layers of different chemical compositions in the crystallographic c-directions.

Dolomites produced in experiments of longer duration are composed of an interstratification of essentially two chemically different dolomite layers, of which the stacking sequence is more perfect than it is at lower crystallization degrees. Both components grow rapidly at the expense of dolomites of intermediate composition. Finally, long-term low-temperature (145 °C) experiments produced two independent, coexistent dolomite phases. Within single dolomite layers cations now lie very close to their theoretical positions. CO_3-tilting and dislocation decreases markedly.

Hydrothermal runs at temperatures > c. 145 °C yielded one single, nearly stoichiometric, highly ordered dolomite phase. Finally, dolomites synthesized at temperatures > c. 200 °C are of an ideal chemical composition and have perfect lattice ordering.

THE formation of dolomites at low temperatures is one of the most interesting questions in sedimentology. The thermodynamic and crystallochemical conditions of dolomite crystallization have been the subject of intensive experimental studies in recent years. Many previous papers have dealt with the investigation of disordered carbonates in natural rocks (Graf and Goldsmith, 1956; Graf *et al.*, 1967; Lippmann, 1973). This paper, based on analyses of synthetic materials, describes stages of dolomite nucleation and crystal growth under the influence of variations in temperature and duration of experiments. The different types of lattice defects and the mode and degree of transformation and ordering processes resulting from this investigation may be useful for further discussion of reaction kinetics and formation conditions of carbonate minerals.

Experimental

CaCl$_2$ and MgCl$_2$ were dissolved in H$_2$O in such a manner that equimolar concentrations of Ca^{2+} and Mg^{2+} ions were present in the solution. After NaHCO$_3$ was added in excess, the solution was evaporated until a precipitate of monohydrocalcite (CaCO$_3 \cdot$H$_2$O) and an amorphous magnesium-rich material was obtained. The precipitate was washed and dried over H$_2$SO$_4$. This material was used for twenty-four hydrothermal runs (standard techniques, see Althaus, 1969) in the temperature range from

90 to 410 °C (accuracy: ± 5 °C) at constant hydrostatic pressure of 500 bar (Table I). Isochemical experiments were carried out with distilled water (sample to water ratio 3 to 1 or 3 to 2) as the starting fluid phase.

TABLE I. *Data for hydrothermal runs*

Run	Temp.	Time	Products	Run	Temp.	Time	Products
1	190°C	28d	**Dol**, Cc, (Bru)	12	145	42	Dol, Cc, (Bru, Arag, Magn)
2	265	28	**Dol**, Cc, (Bru)				
3	330	7	**Dol**, Cc, (Bru)	13	190	7	Dol, Cc, Bru
4	390	21	**Dol**, Cc, (Bru)	14	330	14	**Dol**, Cc, Bru
5	410	21	**Dol**, Cc, (Bru)	15	90	14	*Dol*, Arag, Magn
6	145	14	Dol, Arag, Magn	16	145	3	*Dol*, Arag, Magn
7	145	28	Dol, Cc, (Bru, Arag, Magn)	17	145	5	*Dol*, Arag, Magn
				18	145	$5\frac{1}{2}$	*Dol*, Arag, Magn
8	145	21	Dol, Arag, Magn	19	145	6	*Dol*, Arag, Magn
9	145	7	*Dol*, Arag, Magn	20	145	3	*Dol*, Arag, Magn
10	145	56	Dol, Cc, (Bru)	21	145	2	Arag, Magn
11	165	14	Dol, Cc, (Bru)	22	145	4	*Dol*, Arag, Magn
				23	145	$4\frac{1}{2}$	*Dol*, Arag, Magn
				24	145	119	**Dol**, Cc, (Bru)

Bold type: strong X-ray interferences of dolomite.
Italic type: faint X-ray interferences of dolomite.

Dol = Dolomite; Magn = Magnesite; Bru = Brucite; Cc = Calcite; Arag = Aragonite. Minerals in parentheses show only very faint X-ray reflections.

Results

Reaction products obtained from different hydrothermal runs were investigated by means of X-ray powder methods (film techniques with Guinier-type camera and diffractometer traces; Ni-filtered Cu-$K\alpha$ radiation, Si metal as internal standard); electron microscopy, and infra-red spectroscopy (wavenumber range from 1400 cm^{-1} to 40 cm^{-1}). The precipitate was checked for sodium as well with atomic absorption spectroscopy as with the investigation methods quoted above. No sodium could be detected. A main aim of this investigation was to find a relation between ordering processes and lattice geometry. For this reason, structure factor values $|F|$ of Ca^{2+}, Mg^{2+}, O, and C were calculated for 18 *hkil* planes. Structure factor ratios of $(|F_{Ca} + F_{Mg}|)/(|F_C + F_O|)$ are presented in Table II. The correlation of these ratios to the morphology of individual X-ray lines may be helpful to understand the mode of lattice distortion.

Reaction products. Crystalline phases produced by the different hydrothermal runs are listed in Table I. Low-temperature, short-time experiments essentially lead to the thermodynamically unstable aragonite–magnesite assemblage and to poorly crystallized dolomite (fig. 1). Experiments at temperatures above 145 °C produce dolomite crystals—which become more and more ordered with increasing duration of hydrothermal runs—and small quantities of calcite and brucite (fig. 2).

Lattice parameters and chemical composition of the dolomites. Poorly crystalline dolomites produce only few faint and diffuse X-ray reflections; in many cases only the
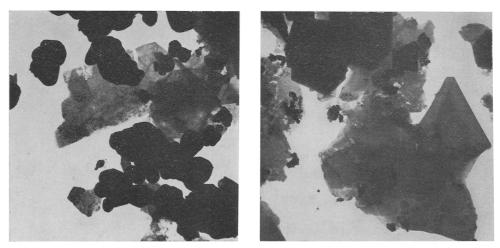
$10\bar{1}4$ peak could be detected. The cation ratios of the dolomites were estimated by means of the $10\bar{1}4$ spacings, following Goldsmith, Graf, and Joensuu (1955). The d-spacings rapidly increase with decreasing synthesis temperatures and/or shorter

TABLE II. *Ratios of the percentage structure factor amounts of individual X-ray reflections* $(|F_{Ca}+F_{Mg}|)/(|F_C+F_O)$

hkil	$\dfrac{(|F_{Ca}+F_{Mg}|)}{(|F_C+F_O|)}$	hkil	$\dfrac{(|F_{Ca}+F_{Mg}|)}{(|F_C+F_O|)}$	hkil	$\dfrac{(|F_{Ca}+F_{Mg}|)}{(|F_C+F_O|)}$	hkil	$\dfrac{(|F_{Ca}+F_{Mg}|)}{(|F_C+F_O|)}$
$10\bar{1}4$	1·13	$01\bar{1}8$	1·69	$11\bar{2}3$	0·42	$12\bar{3}2$	2·45
0006	0·70	$11\bar{2}6$	2·23	$20\bar{2}2$	6·67	$02\bar{2}7$	0·52
$01\bar{1}5$	0·88	0009	0·29	$10\bar{1}7$	0·61	$12\bar{3}5$	0·62
$11\bar{2}0$	59·69	$21\bar{3}1$	0·25	$02\bar{2}4$	22·83	$03\bar{3}0$	3·33

Calculations are based on structure data of Steinfink and Sans (1959).

FIGS. 1 and 2: FIG. 1 (left). Corroded magnesite–aragonite assemblages (dark grains). Transparent inhomogeneous leaflets represent newly formed dolomite crystallites (sample 14, Stage I. Scale: × 8000). FIG. 2 (right). Electron-microscope photograph of relatively well-crystallized dolomite specimen, showing dolomite crystals with rhombohedral (dark) and basal (transparent) forms (sample 11, Stage III. Scale: × 8000).

duration of experiments. If the changing Ca to Mg ratios were the only factor controlling the position of the $10\bar{1}4$ reflection, the corresponding d-values would indicate a ratio 1Ca to 1Mg for perfectly ordered and about 3Ca to 1Mg for poorly crystallized dolomite (Table III). It has to be mentioned, however, that d-values are influenced by structure disorder as well.

Broadening and intensity of individual X-ray lines and their assignment to lattice disordering

A possible correlation was looked for between lattice disorder and the relative line broadening of different X-ray reflections from the same Guinier photograph. Measure-

ments of line broadening were carried out visually with an accuracy of $\pm 0.05°$, 4θ. Percentage line broadenings relative to mean d-values have been calculated for all measurable X-ray reflections; they are presented in figs. 3a–d. Since line broadening is not only controlled by lattice defects, but also by crystal size, the degree of imperfection was correlated with the relative broadenings of different X-ray reflections from the same X-ray film.

TABLE III. *Lattice-spacings and chemical composition of the synthetic dolomites*

Run	$d_{10\bar{1}4}$ range	Cation composition 100 Ca/(Ca+Mg)		Run	$d_{10\bar{1}4}$ range	Cation composition 100 Ca/(Ca+Mg)	
		Range	A			Range	A
1	2·902–2·886 Å	54–50	52	13	2·91–2·88	58–47	51
2	2·902–2·886	54–50	52	14	2·90–2·89	55–51	51
3	2·905–2·884	55–48	53	15	2·93–2·88	65–47	55§
4	2·891–2·882	53–48	50	16	2·95–2·89	72–51	62*
5	2·886		50	17	2·95–2·87	72–44	58§
6	2·93–2·88	65–47	65; 47*	18	2·94–2·88	70–47	65; 55‖
7	2·93–2·88	65–47	65; 55†	19	2·95–2·88	72–47	72; 55‖
8	2·94–2·89	70–51	70; 65†	20	2·94–2·88	70–47	70; 55‖
9	2·94–2·89	70–51	70; 65*	21	2·93–2·87	65–44	55§
10	2·93; 2·91–2·89	65; 58–51	65; 55‡	22	2·95–2·87	72–44	70; 45‖
11	2·91–2·88	58–47	55	23	2·96–2·87	76–44	72; 51‖
12	2·93; 2·92–2·90	65; 62–55	65; 58‡	24	2·94; 2·91–2·89	70–51	65; 55‡

A Intensity maxima of individual X-ray reflections.
* Two weak and diffuse maxima of the X-ray line.
† Two sharp maxima of the X-ray line.

‡ Two independent systems of dolomite reflections.
§ Extremely weak and diffuse X-ray line.
‖ Weak and diffuse X-ray line.

Hydrothermal runs producing dolomites of a similar crystallinity may be classified in five groups corresponding to Stages of progressive lattice ordering:

Stage I. Except 10$\bar{1}$4, no other X-ray reflection could be detected. The intensity of this interference is weak to very weak. Sometimes the intensity distribution shows two weak maxima across the diffraction line. Line broadening and d-values vary markedly from one sample to another, indicating variations both in chemical composition and degree of imperfection of individual dolomite crystallites (Samples: 15, 17, 18, 19, 20, 21, 23, Table IV).

Stage II. More X-ray reflections are observed, but line broadening is still very marked for 10$\bar{1}$4, 11$\bar{2}$3, and 11$\bar{2}$6; 11$\bar{2}$0 and 20$\bar{2}$2 reflections are considerably sharper. Especially 'high l' interferences are markedly diffused; reflection intensities are weak (Samples: 6, 9, 16, Table IV).

Stage III. All dolomite interferences including superstructure reflections are present. The intensities of the X-ray lines are stronger than in the first two stages. Simultaneously, the splitting of some peaks has become more pronounced. 'High l' interferences remain diffuse and broadened (Samples: 7, 8, 11, 13, Table IV).

Stage IV. Hydrothermal runs at T 145 °C produce dolomites of which the X-ray lines are clearly duplicated. With increasing duration of the experiment two complete sets of dolomite X-ray lines at slightly different d-values appear, indicating the
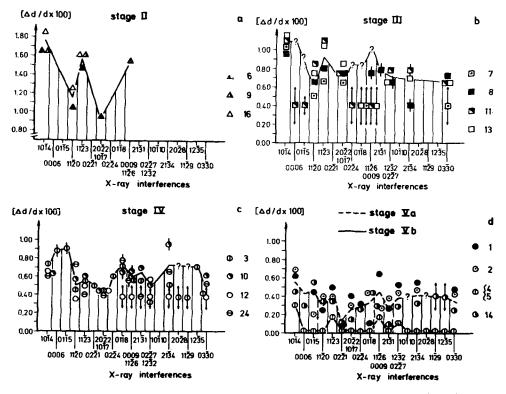

FIG. 3a–d. Percentage line-broadening, $(\Delta d/d) \times 100$, of individual X-ray reflections, dependent on different synthesis temperatures and duration of experiments. Hydrothermal runs with a similar crystallization degree are summarized in five different stages of a progressive crystallization. Line-broadenings of X-ray reflections corresponding to dolomites synthesized at hydrothermal conditions of Stage I are not given, because only the 10$\bar{1}$4 reflections could be detected. In Stage II (fig. 3a) X-ray reflection pairs 20$\bar{2}$2–10$\bar{1}$7 and 0009–11$\bar{2}$6 have to be assigned to 20$\bar{2}$2 and 11$\bar{2}$6, respectively, because 10$\bar{1}$7 and 0009 are superstructure-interferences, which are not to be expected at this crystallization stage. Arrows indicate very diffuse X-ray reflections that could not be measured exactly. d, mean d-spacings; Δd, absolute broadening of individual X-ray lines.

presence of two separate dolomite phases. 'High l' reflections are less diffuse and broadened than they are in Stage III. Relative intensities of individual X-ray inter-ferences are similar to those of well-crystallized dolomites. Experiments at $T > 145$ °C yield only one single, rather well-crystallized phase. (Samples: 3, 10, 12, 24, Table IV.)

Stage V. Intensity data and morphology of individual X-ray reflections are identical to those of well-crystallized dolomites (Samples: 1, 2, 4, 5, 14, Table IV).

The intensity data and morphology of individual X-ray reflections at the several stages are presented in Table IV and fig. 3a–d.

Infra-red spectroscopy

The progress in crystal quality causes some characteristic changes of the infra-red spectra:

At low degrees of crystallinity, the CO_3-libration bands near 160 cm^{-1} show higher intensities than vibration peaks near 260 cm^{-1} and 370 cm^{-1} (Table V). These are assigned to a linear cation bond stretching in (0001), to different CO_3 libration and

TABLE IV. *Intensity data and morphology of individual X-ray interferences dependent on increasing temperature and duration of experiments*

hkil	Stage II		Stage III		Stage IV		Stage V	
	I	M	I	M‡	I	M	I	M
10$\bar{1}$4	w	2m*	s	2m†	vs	—	vvs	—
0006	—	—	vvs	vvd	vw	d	w	—
01$\bar{1}$5	—	—	vw	vvd	w	d	w	—
11$\bar{2}$0	vw	2m*	w	2m†	s	—	s	—
11$\bar{2}$3	w	d§	s	2m†	vs	—	vs	—
20$\bar{2}$2 \ 10$\bar{1}$7	vw	—	w	2m†	w	—	s	—
02$\bar{2}$4	—	—	vw	vd	w	d	w	d
01$\bar{1}$8	—	—	vw	vvd§	w	d	s	—
11$\bar{2}$6 \ 0009	vvw	vvd	w	vvd§	w	—	s	—
21$\bar{3}$1	—	—	w	—	w	—	w	—
12$\bar{3}$2 \ 02$\bar{2}$7	—	—	w	—	w	—	w	—
12$\bar{3}$5	—	—	vvw	vd	vw	d	w	d
03$\bar{3}$0	—	—	w	—	w	—	s	—

I Visually estimated intensities.
M Morphology of X-ray lines.
d diffuse; vd, very diffuse; vvd, extremely diffuse.
‡ Hydrothermal runs at T 145 °C with two independent sets of dolomite X-ray lines.
* X-ray line with two weak and diffuse intensity maxima.
† X-ray line with two sharp intensity maxima.
§ X-ray line broadened towards higher *d*-spacings.

rotation modes, and to translational cation vibrations perpendicular to (0001), respectively (Nakagawa and Walter, 1969; Plihal and Schaack, 1970); 'free' CO_3-librations (*c*. 160 cm^{-1}) are less dependent on cation–carbonate disordering than are movements of cations and carbonate ions against each other (*c*. 260 and 370 cm^{-1}). Together with an extreme broadening of the bands near 260 cm^{-1} and 370 cm^{-1} this may indicate considerably varying cation–carbonate distances and varying Ca/Mg-values in disordered dolomites.

Vibrations within the CO_3-'molecules' (see Adler and Kerr, 1963) are much less strongly influenced by lattice distortions than are the low-energy 'outer' vibration modes. The following CO_3-molecular oscillations can be observed in dolomite: a stretching mode near 720 cm^{-1}, a bending mode at *c*. 870 cm^{-1}, and a stretching mode

at c. 1440 cm^{-1}. The intensity ratios $I(1440)/I(870)$, $I(1440)/I(720)$, and $I(870)/I(720)$ are distinctly higher for disordered than for well-crystallized dolomites. This method seems to be useful for the determination of the degree of order in dolomite (see Table V). With increasing ordering, a shift of the stretching vibration from about 1450 to 1435 cm^{-1} possibly indicates that cation–CO$_3$ distances are enlarged in imperfect lattices. Broad absorption bands near 3500 cm^{-1} suggest the incorporation of some H$_2$O within low-temperature dolomites, but it could not be proved conclusively because of infra-red preparation techniques.

TABLE V. *Intensity-ratios of different infra-red-absorption bands, dependent on the duration of experiment (Temp. const. at 145 °C)*

Duration of experiments	3 days	5½ days	7 days	14 days	28 days	56 days
$\dfrac{I(1440\ \mathrm{cm}^{-1})}{I(870\ \mathrm{cm}^{-1})}$	0·34	0·30	0·19	0·16	0·15	0·13
$\dfrac{I(870\ \mathrm{cm}^{-1})}{I(720\ \mathrm{cm}^{-1})}$	—	—	—	5·77	2·44	2·04
$\dfrac{I(1440\ \mathrm{cm}^{-1})}{I(720\ \mathrm{cm}^{-1})}$	—	—	—	0·94	0·36	0·27
$\dfrac{I(260\ \mathrm{cm}^{-1})}{I(160\ \mathrm{cm}^{-1})}$	—	—	—	0·36	0·66	0·79

Discussion

Short-time, low-temperature experiments (Stage I) with starting material of dolomite bulk composition yield very poorly crystallized dolomite together with metastable aragonite and magnesite by the reaction of calcium carbonate monohydrate with a magnesium-rich material. The difficulty of synthesizing well-crystallized dolomite in this temperature range has been the subject of recent investigations. One reason may be the principle of 'simplexity', which says that 'if the several different types of cation sites do not greatly differ structurally and energetically, cations arriving at improper sites are more likely to be accepted (Graf and Goldsmith, 1956)'. Another reason is a small crystal growth-rate, which is due to the fact that alkaline earth cations, especially Mg^{2+}, are present in aqueous solutions as aquo-complexes. In order to precipitate water-free carbonates from these solutions the hydrate hull must be stripped off the cation; this is not very difficult in case of the relatively large Ca^{2+}-cations, whereas it requires considerable energies to break up the Mg^{2+}(H$_2$O)$_x$ complexes. Preferential incorporation of Ca^{2+} into low-temperature dolomites may be explained in such a way (Lippmann, 1973).

The mechanism of these formation processes has not yet been explained conclusively. It seems feasible that diffusion velocities might be of great importance in dolomite formation. Since the diffusion velocities in solutions are higher for Ca^{2+} ions than for Mg^{2+}(H$_2$O)$_x$ complexes, dolomite nuclei may be surrounded by a layer of the solution,

enriched in $Mg^{2+}(H_2O)_x$. Cation diffusion rates to the dolomite crystallites may be controlled by the 'density' of these layers, e.g. its permeability to ion movings. This density probably is strongly dependent on temperature, pressure, and chemical composition of the fluid phase. Low temperatures, for example, favour the formation of $Mg^{2+}(H_2O)_x$ layers and so delay the further growth of the dolomites, whereas at higher temperatures the layers are decomposed, leading to a rapid crystal growth.

Dolomites produced by longer lasting hydrothermal runs, corresponding to Stage II, are still strongly disordered. However, $11\bar{2}0$ and $20\bar{2}2$ reflections are relatively sharp. This might indicate a higher degree of order within lattice planes perpendicular—or nearly perpendicular—to the c-axis. If this assumption is correct the main ordering directions may be densely packed lattice rows with short translation vectors in (0001). The shortest Burgers vectors in (0001) are $\langle 10\bar{1}0 \rangle$ (length: 4·81 Å) and $\langle 11\bar{2}0 \rangle$ (length: 4·81 Å). They link cations or CO_3 groups, respectively. The observed X-ray properties so suggest a relatively good ordering of Ca^{2+} and Mg^{2+} in very small crystal domains. A random succession of such domains, however, produces a long-range mosaic-type disorder, responsible for the lack of the superstructure reflections.

Additional structure defects may be caused by irregular dislocation and tilting of the CO_3-groups. This is inferred from the breadth of 'high l' reflections, which are characterized by a high contribution of the CO_3-molecules to the structure amplitude (e.g. low $(|F_{Ca}^{2+}+F_{Mg}^{2+}|)/(|F_C+F_O|)$-ratios; Table II). This type of lattice imperfection may be increased by water absorption at the edges of the lattice defects, as is suggested by infra-red investigations.

The chemical compositions of the low-temperature dolomite-like phases are estimated from their X-ray properties (see above). They indicate variations within the same sample ranging maximally from $Ca_{0.44}$ to $Ca_{0.72}$, mostly with two maxima between $Ca_{0.55}$ to $Ca_{0.60}$ and between $Ca_{0.65}$ to $Ca_{0.70}$, respectively. Together with the extreme diffuseness of 'high l' reflections, these properties suggest that dolomite layers of essentially two different chemical compositions are stacked randomly in the crystallographic c-direction leading to a high degree of stacking disorder. In some respect, these phases therefore resemble mixed layer phases of sheet silicates (see also Graf, Blyth, and Stemmler, 1967; Lippmann, 1973).

Electron-microscope photographs (figs. 1 and 2) show that the dolomite crystals are sometimes very thin leaflets ($< c.$ 500 Å) parallel to (0001). The Fourier transformation of the l-interferences in the reciprocal space are lattice rods parallel to [0001]. This particular crystal habit may sometimes be responsible for broad and diffuse 0001 X-ray reflections as well as disorder phenomena.

Experimental runs of higher temperature or longer duration (Stage III) yield dolomites producing X-ray patterns of much better quality than those of Stages I and II. The presence of weak superstructure reflections demonstrates that the domains with higher ordered cation distributions have been distinctly enlarged. The dolomite crystallites are now essentially composed of two components, of which the cation composition varies between $Ca_{0.55}$ and $Ca_{0.65}$ and between $Ca_{0.65}$ and $Ca_{0.70}$. With increasing duration of experiments both components form rapidly growing domains within the carbonate lattice. Long-time experiments carried out at 145 °C (Stage IV)

finally produce two independent phases with two sets of X-ray reflections at slightly different d-values. The chemical composition of one phase ranges between $Ca_{0.53}$ and $Ca_{0.58}$; the other is near $Ca_{0.65}$. Intensive superstructure lines suggest the growth of well-ordered cation domains. They lead to cation layers consisting essentially of either calcium or magnesium. Within these layers the cations lie very close to their theoretical positions: this is inferred from the occurrence of sharp X-ray reflections to which the cations make a marked contribution ($02\bar{2}1$, $03\bar{3}0$). Hydrothermal runs at temperatures $>c.$ 145 °C yield only one single stoichiometric, highly ordered dolomite phase. Finally, dolomites synthesized at temperatures $>c.$ 200 °C—corresponding to Stage V—are of ideal chemical composition and have nearly perfect lattice ordering.

Data on the ordering mechanism of low-temperature dolomites as presented in this paper will be completed by detailed investigations of the reaction kinetics.

REFERENCES

ADLER (H. H.) and KERR (P. F.), 1963. *Amer. Min.* 48, 839–53.
ALTHAUS (E.), 1969. *Neues Jahrb. Min. Abh.* 111, 74–110.
FÜCHTBAUER (H.) and MÜLLER (G.), 1970. *Sedimente und Sedimentgesteine.* Stuttgart (Schweizerbart).
GOLDSMITH (J. R.), GRAF (D. L.), and JOENSUU (O. J.), 1955. *Geochimica Acta,* 7, 212–30.
GRAF (D. L.), 1961. *Amer. Min.* 46, 1283–1316.
—— 1969. Ibid. 54, 325.
—— BLYTH (C. R.), and STEMMLER (R. S.), 1967. *Illinois State Geol. Survey Circ.* 408.
—— and GOLDSMITH (J. R.), 1956. *Journ. Geol.* 64, 173–86.
LIPPMANN (F.), 1973. *Sedimentary carbonate minerals.* Berlin–Heidelberg–New York (Springer).
NAKAGAWA (I.) and WALTER (J. L.), 1969. *Journ. Chem. Phys.* 43, 1389–97.
PLIHAL (M.) and SCHAACK (G.), 1970. *Phys. stat. solids,* 42, 485–96.
STEINFINK (H.) and SANS (F. J.), 1959. *Amer. Min.* 44, 679–82.